**Solid Freeform Fabrication 2019: Proceedings of the 30th Annual International Solid Freeform Fabrication Symposium – An Additive Manufacturing Conference**
**Reviewed Paper**

# An Automated Method for Geometrical Surface Characterization for Fatigue Analysis of Additive Manufactured Parts

Behnam Rasoolian[1*], Jonathan Pegues[2,3], Nima Shamsaei[2,3], Daniel Silva[1,3]

[1]*Department of Industrial and Systems Engineering, Auburn University, Auburn, AL 36849*

[2]*Department of Mechanical Engineering, Auburn University, Auburn, AL 36849*

[3]*National Center for Additive Manufacturing Excellence (NCAME), Auburn University, Auburn, AL 36849*

**Corresponding author:*

*Tel: 334-439-9588*

*Email: behnam@auburn.edu*

## Abstract

Recent interest to implement additive manufactured parts into structural applications has created a critical need to better understand the fatigue behavior of these parts. Alloys such as Ti-6Al-4V are popular in the aerospace and biomedical industries due to their superior strength to weight ratio and biocompatibility. Previous works have associated fatigue behavior with surface roughness, especially radius of curvature of notches. It is therefore important to develop a fast, reliable and consistent methodology for extracting such curvatures. The contribution of this paper is in providing an automated method for extracting radius of curvature using image processing techniques and optimization. Results on fatigue life prediction indicates similar results between the automated method and manually extracted radii in a significantly shorter period of time.

**Keywords:** Additive manufacturing, Fatigue behavior, Roughness, Radius of curvature

# Introduction

Additive manufacturing has become an increasingly popular technique to produce structural parts or components. In particular, additive manufacturing has gained a significant amount of interest in aerospace and biomedical sectors with Ti-6Al-4V alloy being prominently used in both these industries. The popularity of titanium alloys is due to their high strength to weight ratio, biocompatibility, excellent corrosion resistance, and general weldability. Studies have shown that variations in surface roughness can have significant effects on the fatigue resistance of laser beam powder bed fused (LB-PBF) metallic parts such as Ti-6Al-4V [1, 5].

Pegues. et. al. [6] proposed an approach for estimating the effect of surface roughness on the fatigue strength of additive manufactured Ti-6Al-4V using an approximation of the fatigue notch factor, which was previously used to incorporate roughness in fatigue life in [7]. The fatigue notch factor is expressed by the following equation:

$$\bar{K}_f = 1 + \frac{n(\frac{R_a}{\bar{\rho}_{10}})(\frac{R_t}{R_{zISO}})}{1+\frac{\gamma}{\bar{\rho}_{10}}} \quad (1)$$

where $n$ accounts for changes in stress state ($n = 1$ for shear and $n = 2$ for tension), $\gamma$ is a material characteristic length [3] and $R_a$, $R_t$, $R_{zISO}$, and $\bar{\rho}_{10}$ are mean roughness, max peak-to-valley roughness, 10-point height roughness, and 10-point valley radii respectively. For the results in [1] n = 2 was used for the stress state and g was considered as the average acicular grain width of 1.5 μm. The surface roughness parameters are calculated using Equations 2-5:

$$R_a = \frac{1}{l}\int_0^l |y| \quad (2)$$

$$R_t = |y_{max} - y_{min}| \quad (3)$$

$$R_{zISO} = \frac{1}{5}[\sum_{i=1}^{5} y_{i-max} + \sum_{j=1}^{5} y_{j-min}] \quad (4)$$

$$\bar{\rho}_{10} = \frac{1}{5}[\sum_{j=1}^{5} \rho_{j-min}] \quad (5)$$

In Equation (5), $\rho_{j-min}$ are the radii of the five deepest valleys. In order to completely analyse the effect of roughness on fatigue, these radii should be calculated for all roughness profiles. A typical surface roughness image can consist of hundreds to thousands of such profiles, making the measurements of these radii extremely cumbersome, if not impossible. An automated method is therefore desired not only to improve the time it takes to extract radii, but also to provide objective, reliable and consistent results that don't depend on individual judgements.

In this paper, we propose an objective, consistent, automated technique for extracting each radius of curvature of valleys as described in the proceeding section. The method significantly reduces the time it takes to find the radii, while providing results that are comparable to manually computed radii. The proposed technique is aimed at reducing the time to manually measure the surface characteristics while improving the repeatability of the calculations to obtain accurate and consistent roughness measurements. These results can then be used as inputs for models that predict mechanical properties. Using an objective, repeatable method to calculate the inputs allows researchers to compare different models fairly.

## Methods

Given a surface roughness profile containing point height data, obtained e.g. through microscopy, our method extracts radii of curvature for valleys. This is done by approximating the radius of curvature at the base of a valley which can be considered a local minimum in the roughness profile. Radius of curvature ($R$) of a curve at point $x$ can be analytically computed using the following equation:

$$R = \left| \frac{(1+f'(x)^2)^{\frac{3}{2}}}{f''(x)} \right| \qquad (6)$$

Where $f'(x)$ and $f''(x)$ are first and second derivatives of the curve at point $x$. Note that if $x$ is a local minimum (or maximum), $f'(x) = 0$ and the above formula turns into $R = \left|\frac{1}{f''(x)}\right|$. In a noisy roughness profile, computation of radius of curvature using $f'$ and $f''$ values computed numerically is highly unstable and prone to numerical errors since a roughness profile is provide as a discrete set of data points and values of $f'$ and $f''$ can change significantly from one data point to and adjacent point. Therefore, there is a need for a more robust method that can be adapted to various roughness profiles.

In this work, the computation of valley radii is done in three steps: In the first step, profiles are smoothed and the coordinates of local minima $(x_i, y_i)$ are extracted as valleys. A 1-dimensional Gaussian kernel is used for smoothing. The size of the kernel is determined as a fraction (one fifth) of the average valley widths. The valley widths are determined as the distance between the beginning and the end of the valley that is below one standard deviation of the mean roughness. These local minima are then filtered such that only the lowest ones are chosen. The criterion for filtering is that a point is dropped if $y_i > R_a - \sigma_y$ where $\sigma_y = \sqrt{\frac{1}{l}\int_0^l (y - R_a)^2}$ is the standard deviation of the profile. We denote $M$ as the set of all valleys that are selected in this step. This process is illustrated in Fig. 1. The valley widths are depicted using black lines. The Gaussian smoothing kernel and the neighborhood from which the local minima are extracted both use kernels sizes that are one fifth of average valley widths. We denote this kernel size with $l$.

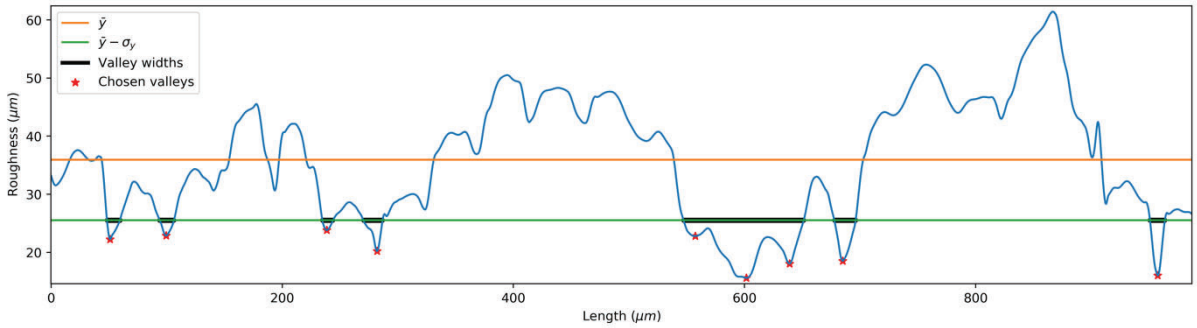


*Figure 1: Valley local minima (valleys) that fall below one standard deviation of average roughness in a roughness profile.*

In the second step for each valley in $M$ a neighborhood is chosen for fitting a circle. This is done by finding the nearest inflection points, that is, the point that the second derivative of the profile changes sign, on the two sides of the valley. This neighborhood ensures that a concave set of points are used to fit a circle. In order to guarantee that the neighborhood is symmetric relative to the local minima, the shorter distance from the two inflection points is chosen and mirrored to the other side of the valley (local minima). The neighborhood size normally does not exceed the size of the kernel used to find the local minima ($l$). In rare cases where this happens the neighborhood is shrunk to have size $l$ ($\frac{l}{2}$ on either side of the local minimum). Fig. 2 illustrates the process of choosing the neighborhood. We let $N_i$ denote the points that comprise a neighborhood of the $i$-th valley in $M$.

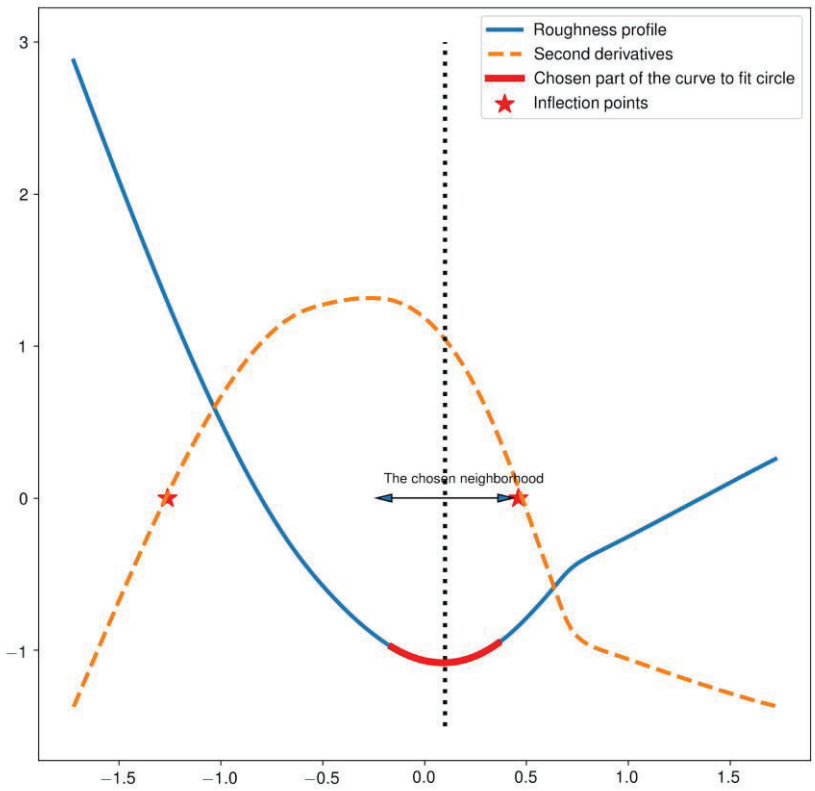


*Figure 2: Process of choosing a neighborhood for a typical valley. In order to maintain symmetry, the closest inflection point to the local minimum is chosen (in this case the inflection point that is to the right) and mirrored on the other side of the minimum.*

Finally, for each valley $i$, a circle is fit to the points in $N_i$. In order to account for different scales and keep numerical stability, the points in $N_i$ are first normalized into $N_i'$. A circle is then fit to the normalized points and the resulting circle is transformed back to an ellipse in the scale of data points. Finally, the radius of curvature of the data points is computed by finding the radius of

curvature at the base of the transformed ellipse. The rest of this section provides more detail on this process and provides illustrated examples of results obtained by following this methodology.

Normalization of points in $N_i$ is done using the following formulae:

$$x'_{ij} = \frac{x_{ij} - \bar{x_i}}{\sigma_{x_i}}, \quad y'_{ij} = \frac{y_{ij} - \bar{y_i}}{\sigma_{y_i}} \tag{7}$$

Where $\bar{x_i}$ ,$\bar{y_i}$ are means of the coordinates of the points in $N_i$ and $\sigma_{x_i}$ and $\sigma_{y_i}$ are standard deviations of the points.

The circles are then found by minimizing an objective function $f(c_{xi}, c_{yi}, r_i)$ where $(c_{xi}, c_{yi})$ is the center of the circle and $r_i$ is its radius. The function is expressed by the following equation:

$$f(c'_{xi}, c'_{yi}, r'_i) = \frac{1}{|N'_i|} \sum_{(x'_{ij}, y'_{ij}) \in N_i} \sqrt{{r'_{ij}}^2 - {r'_i}^2} + \lambda t_{ij} \tag{8}$$

where ${r'_{ij}}^2 = (x'_{ij} - c_{,xi})^2 + (y'_{ij} - c_{,yi})^2$ and $\lambda t_{ij}$ is a penalty term which forces the circle perimeter to align with curve points as opposed to having points inside the circle. $t_{ij}$ is 0 if $r'_i < r'_{ij}$ and 1 otherwise and $\lambda$ is a large (>500) penalty coefficient. Non-linear optimizers, such as gradient descent can be used in order to find optimal values of $c'_{xi}$, $c'_{yi}$, and $r'_i$.

$c'_{xi}$, $c'_{yi}$, and $r'_i$ are fit to the scaled transformations of the points in $N_i$ and need to be transformed back to the same scale as the points in $N_i$. This is done by performing the following transformation:

$$c_{x_i} = c'_{x_i} \times \sigma_{x_i} + \bar{x_i}, \tag{9}$$

$$c_{y_i} = c'_{y_i} \times \sigma_{y_i} + \bar{y_i}, \tag{10}$$

$$r_i = r'_i \times \frac{\sigma_{x_i}^2}{\sigma_{y_i}} \tag{11}$$

Note that the result of transforming the circle $(c'_{x_i}, c'_{y_i}, r'_i)$ back to scale is not a circle but an ellipse whose center is at $(c_{x_i}, c_{y_i})$ and its radii are $(r'_i \times \sigma_{x_i}, r'_i \times \sigma_{y_i})$. The radius of curvature at the base of an ellipse with radii $(r_1, r_2)$ is $\frac{r_1^2}{r_2}$. Plugging in $r'_i \times \sigma_{x_i}$, $r'_i \times \sigma_{y_i}$, leads to equation 11.

Results of the automated extraction method for a single profile are illustrated in Fig. 3, where four sections of a roughness profile are plotted along with the circles fit on the deepest valleys. It can be observed that the extraction method successfully locates the deepest valleys from each profile. To illustrate how the method works on a wide variety of profiles, radii extractions for several different profiles are provided in Appendix I.

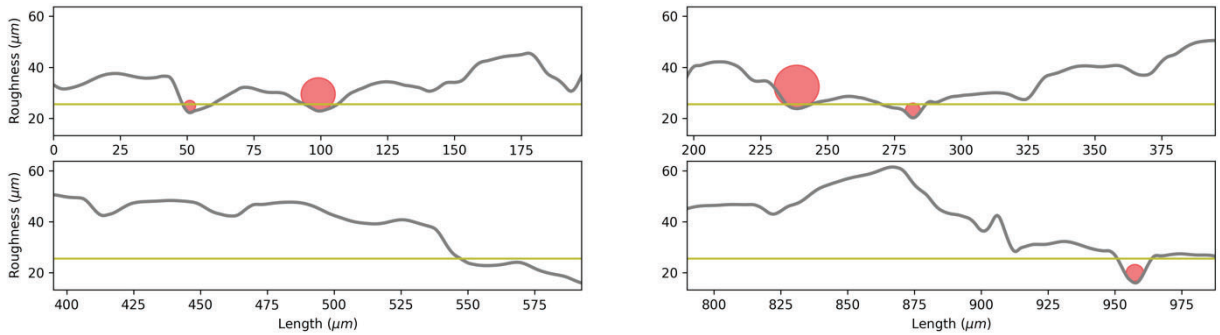


*Figure 3: Valley radii for a roughness profile. The golden horizontal line separates the valleys that are one standard deviation below $\bar{y}$.*

## Experimental Results

The proposed method of fitting circles was tested on local minima of randomly generated polynomial curves of degrees 2 and 3. For each polynomial degree, 1000 expressions were generated using coefficients that were randomly generated from values between 0 and 100. For example, to generate a single random polynomial of the third degree, 4 coefficients $a, b, c,$ and $d$ were randomly generated and the expression $ax^3 + bx^2 + cx + d$ evaluated. The radius of circles extracted was then compared to analytically computed radius of curvature at the local minima that were computed using the formula $\frac{1}{f''^2(x)}$ where $x$ is the location of the minima. The relative error was then measured. For polynomials of the third degree, the mean relative error was 0.0836 with standard deviation of 0.0893 and for polynomials of the second degree, mean relative error was 0.0166 with standard deviation of 0.0016. These results show that the fit circles are highly reliable measures of radius of curvature.

The fatigue life estimations by Pegues et al. were reproduced using automatically extracted valley radii. In that paper, the authors provided fatigue life predictions of the endurance limit, using $\bar{K}_f$ (as defined in Equation 1), for two sets of roughness geometries, denoted AB1 and AB2. Using basic machine design principles, the authors then estimated the fatigue strength at 1000 cycles which has been traditionally used to signify the transition from low cycle to high cycle fatigue. A straight line fit in log-log coordinates is then constructed to estimate the stress-life curve. The important thing to note here is that only the smooth surface finish endurance limit, ultimate tensile strength, grain size, and roughness parameters are used to estimate the stress-life curves and that no fatigue data from the as-built surfaces are used in the predictions. Comparing the prediction curves with results from the destructive tests, it can be observed that the curve is slightly non-conservative. However, the predictions give reasonable results which, coupled with appropriate safety factors, may be useful in design given no available fatigue results are obtainable.

A comparison of the predictions from the automated method and predictions of the original, manual method are demonstrated in Fig. 4. Graphs of the same color are predictions of fatigue life for parts with the same roughness geometries, with the dashed line corresponding to the manual method and solid lines corresponding to the automated method. Table 1 provides quantitative comparisons of the two methods in terms of mean squared errors (MSE) of the predicted fatigue life from the actual observations. As can be seen, the automated method can provide an accurate and reliable alternative for manually extracted radii in prediction of fatigue life. For both surface

conditions, the automated method closely matches the results of the manual method. Furthermore, the automatic approach moves the predictive line closer to the fatigue data. The higher accuracy can be due to the fact that the automated method used a larger number of profiles to obtain valley radii. However, additional experiments are required to determine whether one method is consistently more accurate than the other. We can conclude that this approach can significantly reduce the time to obtain the radii measurement while also reducing the ambiguity inherent to manually measuring each radius.

*Figure 4: A comparison of fatigue life computations from Pegues et al. and the automated method proposed herein.*

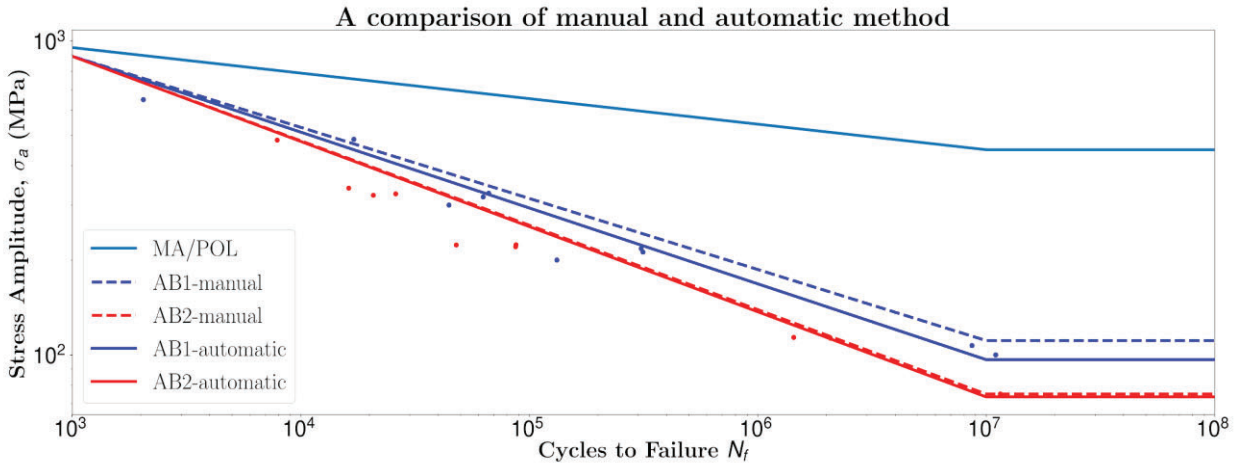


*Table 1: A quantitative comparisons of the manual and automatic methods of radii extraction using minimum squared errors*

| | Automatic method | Manual method |
|---|---|---|
| AB1 MSE | 1883 | 3042 |
| AB2 MSE | 2547 | 2774 |

## Conclusions

In this study, an automated approach is developed for predicting the effect of surface roughness on fatigue failure by analyzing surface roughness in metallic parts. Surface data is collected using digital focal variation microscopy and the standard roughness parameters along with geometrical parameters are automatically extracted. The results are then used to estimate the effective stress concentration and fatigue notch factors for the AM surfaces, using the model proposed in [1]. Results show that fatigue life predictions using the automated method are comparable to results from manually extracted radii. The proposed extraction method can not only reduce the time costs required for manual measurements but, more importantly, also remove judgement element from the measurement, ensuring repeatability in the results despite the operator performing the experiments.

## References


[1] J. Pegues, M. Roach, R. S. Williamson, and N. Shamsaei, "Surface roughness effects on the fatigue strength of additively manufactured Ti-6Al-4V," *Int. J. Fatigue*, vol. 116, pp. 543–552, 2018.

[2] J. Gockel, L. Sheridan, B. Koerper, and B. Whip, "The influence of additive manufacturing processing parameters on surface roughness and fatigue life," *Int. J. Fatigue*, vol. 124, pp. 380–388, 2019.

[3] A. Yadollahi and N. Shamsaei, "Additive manufacturing of fatigue resistant materials: Challenges and opportunities," *Int. J. Fatigue*, vol. 98, pp. 14–31, 2017.

[4] D. Greitemeier, C. Dalle Donne, F. Syassen, J. Eufinger, and T. Melz, "Effect of surface roughness on fatigue performance of additive manufactured Ti–6Al–4V," *Mater. Sci. Technol.*, vol. 32, no. 7, pp. 629–634, 2016.

[5] H. Neuber, *Theory of notch stresses,* Springer-Verlag, Berlin, 1958.

[6] J. W. Pegues, N. Shamsaei, M. D. Roach, and R. S. Williamson, "Fatigue life estimation of additive manufactured parts in the as-built surface condition," *Mater. Des. Process. Commun.*, p. e36, 2019.

[7] D. Arola and M. Ramulu, "An examination of the effects from surface texture on the strength of fiber reinforced plastics," *J. Compos. Mater.*, vol. 33, no. 2, pp. 102–123, 1999.

**Appendix I:** Further examples of radii extraction on different profiles:

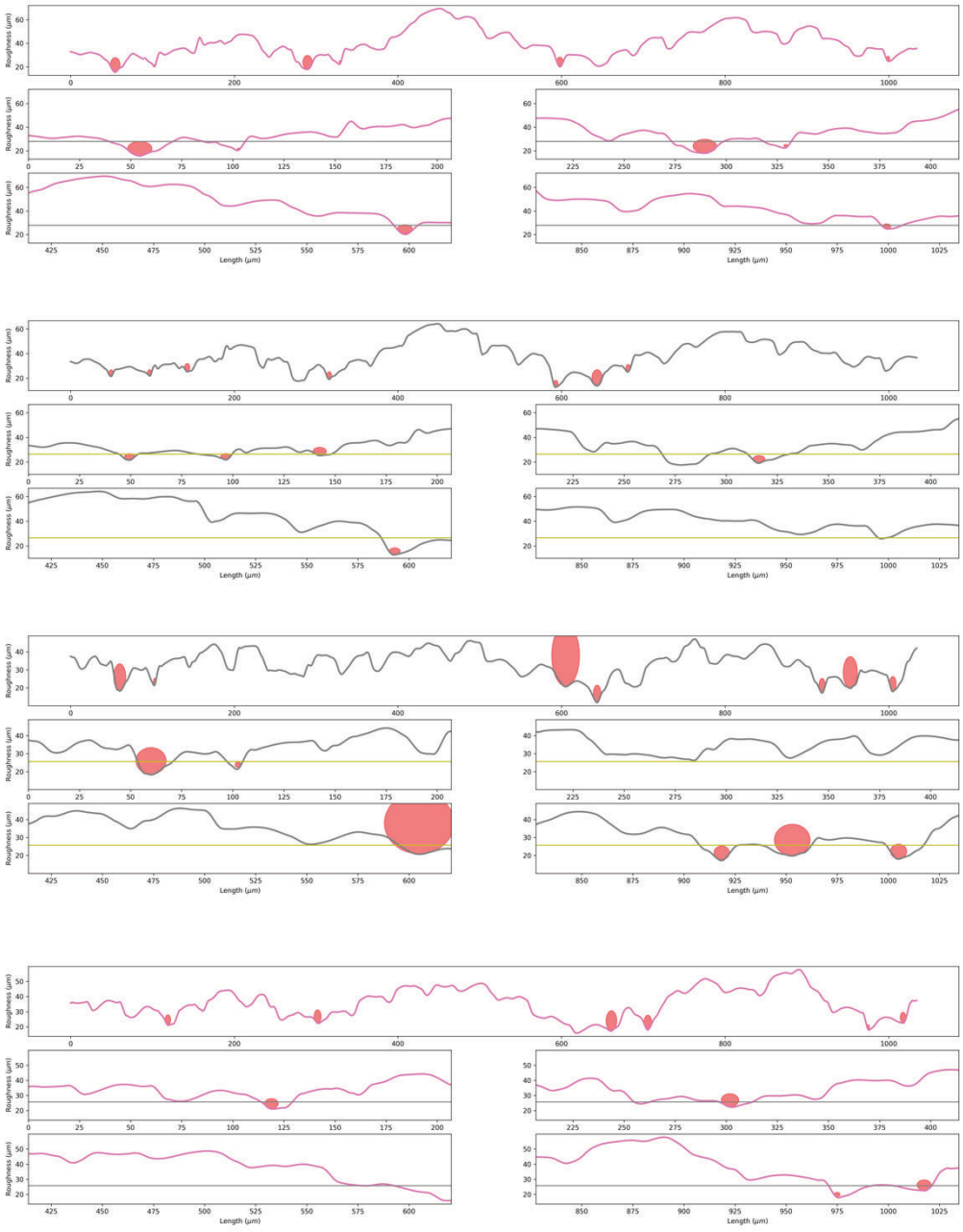

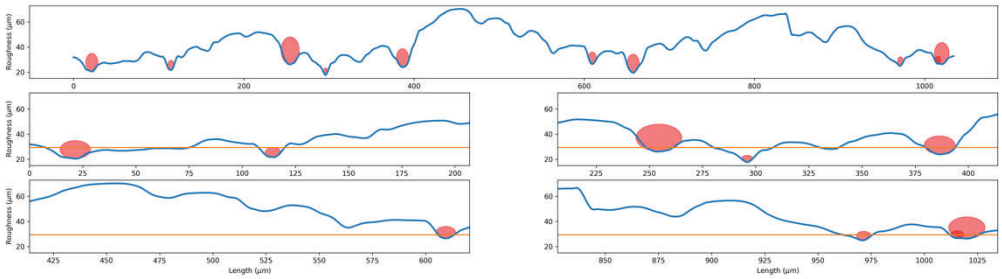
Roughness (μm)
Length (μm)

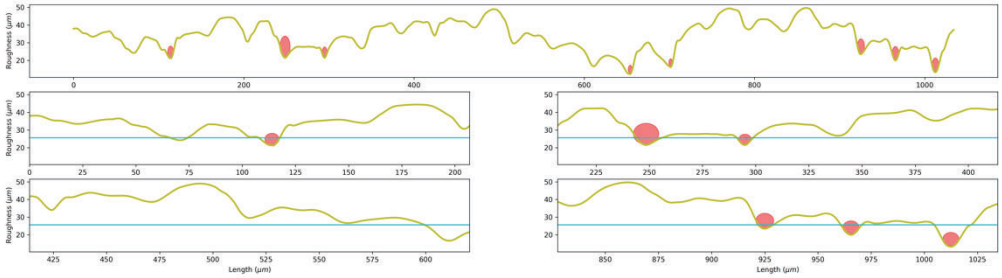
Roughness (μm)
Length (μm)

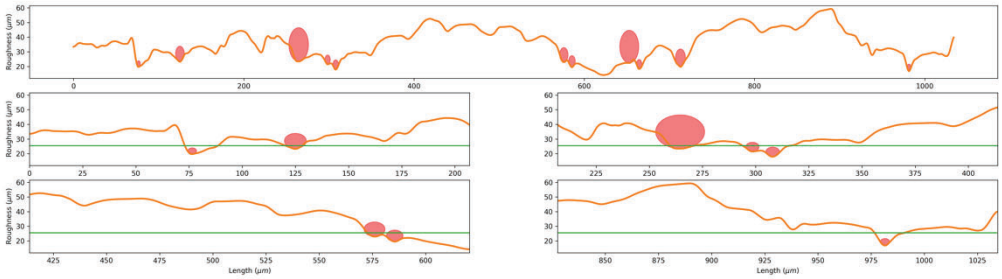
Roughness (μm)
Length (μm)

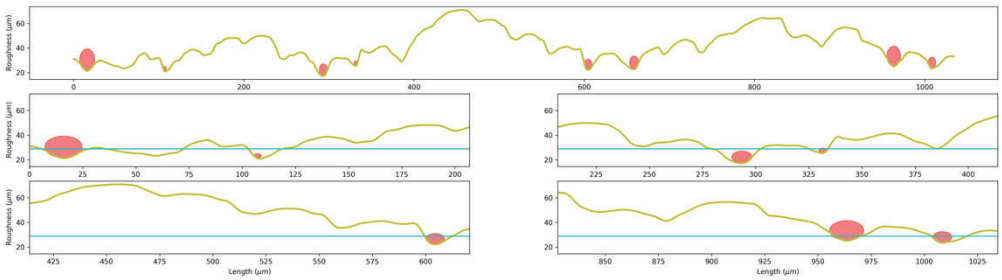
Roughness (μm)
Length (μm)

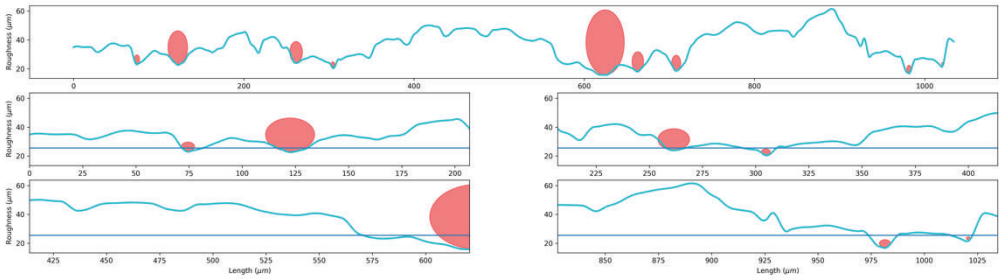
Roughness (μm)
Length (μm)

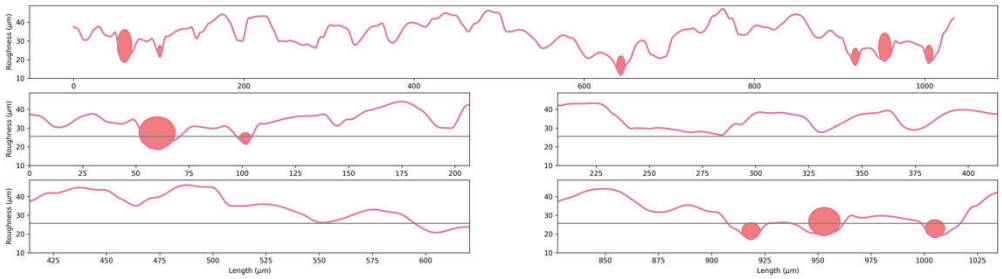
Roughness (μm)
Length (μm)